
Radical Kinetics in Sub- and Supercritical CO₂: Thermodynamic Rate Tuning

Muons stop in the fluid, after passing through a counter and starting a fast electronic clock, forming muonium or residing in a diamagnetic state. The fraction of spin-polarized muons in muonium, diamagnetic or lost polarization fractions is largely dependent on the density of CO₂ for a particular experiment.^[S1] The muon decays with a mean lifetime of 2.2 μs into a positron and an undetected electron neutrino muon antineutrino pair. The positron is emitted asymmetrically with respect to the muon spin vector and is directionally dependent on the remnant muon spin-polarization and positron energy. Detection of the positron from a surrounding counter stops the fast electronic clock and the signal is converted to a time differential to be placed into an incremented histogram bin number. Decay histograms have the form

$$N(t) = N_0[\exp(-t/\tau_\mu) + b][1 + A(t)] \quad (1)$$

where N_0 is a normalization factor, τ_μ is the mean muon lifetime, b is the contribution of background decay events, and $A(t)$ is the muon asymmetry. Asymmetry describes the time evolution of muon spin-polarization of all possible diamagnetic or paramagnetic muon environments, expressed as

$$A(t) = \sum_i A_i \exp(-\lambda_i t) \cos(\omega_i t + \phi_i) \quad (2)$$

where A_i is the asymmetry of the fraction i , λ_i is the relaxation rate, ω_i is the frequency, and ϕ_i is the fraction's initial phase. Parameters A_i , λ_i , and ω_i corresponding to the muonium fraction are extracted from fits to experimental spectra and respectively convey details of muonium formation, kinetics, and hyperfine interactions. Run times were 1–2 hours, depending on the thermodynamic conditions of the experiment, and the corresponding optimally tuned muon-beam momentum.

Rate constants were determined from

$$k = \frac{\lambda - \lambda_0}{[\text{VDF}]} \quad (3)$$

where k is the second order rate constant for ^{0.11}H + VDF, λ is the observed muonium relaxation rate, λ_0 is the background relaxation rate of muonium in CO₂, and [VDF] is the concentration of VDF. Relatively low concentrations of VDF were used to keep reaction rates on a measureable timescale for TF-μSR, ranging 0.07 to 1.21 mmol L⁻¹. For observation of product free radicals at larger TF magnetic fields we used a concentration of ~1 mol L⁻¹.

A high temperature and pressure (HTP) setup was used to house and transfer the gaseous reagents to the target cell. The HTP setup was assembled with the target mounted in the centre of TRIUMF's 'Omni-Prime' μSR spectrometer. Target cell specifications are given elsewhere.^[S2] Transverse magnetic fields of about 6 G were applied vertically via Helmholtz coils. A two-counter system in the plane of precession was arranged on the left and right sides of the target cell [only a single counter setup is shown in Fig. 1 (A) for clarity]. Counters consisted of plastic scintillator pairs, which were taken in coincidence.

CO₂ fluid properties for each experiment were calculated from measured temperatures and pressures using the NIST REFPROP® application and its recommended equation of state (EOS) for CO₂.^[S3]

Primary Muoniated VDF Radical

The primary muoniated radical product was determined through a two-fold approach: (1) under conditions of increased VDF concentrations ($\sim 1 \text{ mol L}^{-1}$) TF- μ SR was used to observe the muoniated radical product and measure its isotropic muon hyperfine coupling constant (HFCC) for comparison with computed values from theoretical chemical models; (2) all possible $^{0.11}\text{H} + \text{VDF}$ reaction channels were modelled computationally for comparison of their relative kinetics. The Gaussian 09® software package^[S4] was used for all computations. All frequency calculations have been done with mass of muon instead of proton for muoniated species.

(1) The computed values for isotropic muon HFCC for radical products corresponding to muonium addition to either VDF's protonated or fluorinated carbon were investigated using with the B3LYP model chemistry^[S5] and the EPR-III basis set.^[S6] Values of isotropic muon HFCC for either radical were determined from the Boltzmann weighted averages of the muon HFCC for the rotational conformations at local energy minima on their potential energy surface (PES). Tab. S1 lists computed HFCCs with conformational energies and Tab. S2 give the corresponding optimized geometries. Fig. S1 compares the UB3LYP/EPR-III computed muon HFCCs with the experimentally determined muon HFCCs. The methodology for extracting experimental muon HFCCs is given elsewhere.^[S7] The computed isotropic muon HFCC for the muoniated radical corresponding to addition to the protonated carbon on VDF agrees with experimentally observed HFCCs in CO₂ to within a 6 MHz mean absolute deviation. Conversely, a minimum deviation of 21 MHz is found for our model representing the radical corresponding to muonium addition to VDF's fluorinated carbon.

(2) The $^{0.11}\text{H} + \text{VDF}$ reaction was modelled computationally to help determine its kinetically preferential reaction channel. Based on accounts from the literature^[S8-S10] and from successful computationally optimized reaction pathways, four reaction channels were determined: **A** – addition to VDF's protonated carbon; **B** – addition to VDF's fluorinated carbon; **C** – hydrogen atom abstraction; and **D** – fluorine atom abstraction. Tables S3 and S4 outline the optimized geometries and thermal activation parameters for each channel using the B3LYP,^[S5] Hartree-Fock,^[S11-S13] second-order Møller-Plesset^[S14-S19] model chemistries, and the large 6-311++G(3df,3dp) Pople basis set. All values are for standard state conditions in the gas phase. Relative rate constants were estimated using free energies of activation (ΔG^\ddagger) and the appropriate expression for bimolecular reactions following transition state theory (TST).^[S20] The extent of tunnelling effects were not pursued or included in estimated rate constants. Each model chemistry favours channel **A**, whose free energy barrier is $\sim 20 \text{ kJ mol}^{-1}$ less than the next least-energy pathway (channel **B**). Differences in the estimated relative rate constants suggest that our observed rate should be for path **A** and that the contribution from other pathways should be insignificant.

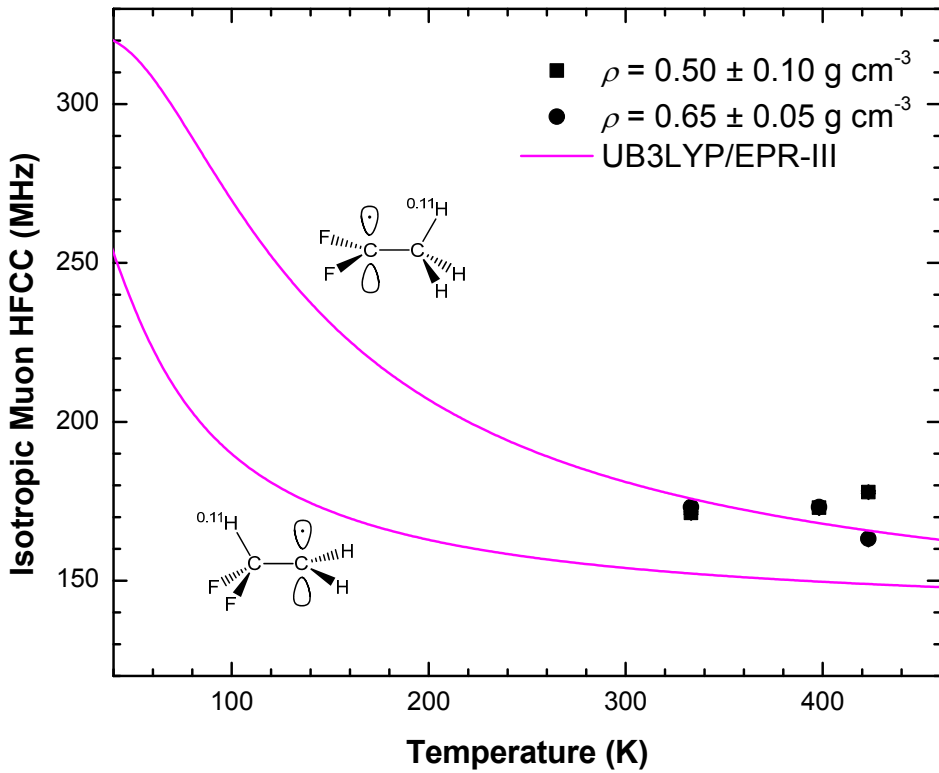


Figure S1. Temperature dependence of the muoniated VDF radical muon HFCC. It should be noted that our optimized geometry for the CH_3CF_2 radical (table S2) is not planar and the above schematic drawings are simple ChemDraw pictures for ease of comparison of the two free radicals.

Table S1. Computed isotropic muon hyperfine coupling constants for the primary muoniated VDF radical's three stable rotational conformations using the UB3LYP/EPR-III method and basis set. E includes ground state electronic and zero-point vibrational energies.

n_i	$\text{CH}_2^{0.11}\text{H}-\text{CF}_2$		$\text{CH}_2-\text{CF}_2^{0.11}\text{H}$	
	A_μ (MHz)	E (hartree)	A_μ (MHz)	E (hartree)
1	322.39414	-277.711135	287.720672	-277.701679
2	34.35116	-277.710441	61.807296	-277.701374
3	34.35144	-277.710441	61.807296	-277.701374

Table S2. Optimized geometries of the two possible muoniated VDF radicals using the UB3LYP model chemistry and the EPR-III basis set.

$\text{CH}_2^{0.11}\text{H}-\text{CF}_2$					$\text{CH}_2-\text{CF}_2^{0.11}\text{H}$				
	n_i	X	Y	Z	n_i	X	Y	Z	
1	C1	-1.390365	0.000000	0.045400	1	C1	1.398960	0.000019	-0.085726
	H2	-1.867894	-0.887210	-0.365537		H2	1.920989	-0.937911	-0.191928
	H3	-1.867894	0.887210	-0.365536		H3	1.920699	0.938006	-0.192839
	Mu4	-1.522997	-0.000001	1.134442		C4	-0.013564	-0.000011	0.340162
	C5	0.054079	0.000000	-0.302207		Mu5	-0.158175	-0.000078	1.427110
	F6	0.737583	1.093638	0.063193		F6	-0.666445	1.108777	-0.142670
	F7	0.737584	-1.093638	0.063193		F7	-0.666432	-1.108784	-0.142771
2	C1	-1.390365	-0.000001	0.045400	2	C1	-1.398218	-0.086933	-0.088918
	H2	-1.867893	-0.887212	-0.365537		H2	-1.622429	-0.555875	-1.035118
	Mu3	-1.867895	0.887208	-0.365536		H3	-2.172648	0.418327	0.466929
	H4	-1.522997	-0.000003	1.134442		C4	0.003643	0.006212	0.354861
	C	0.054079	0.000000	-0.302207		F5	0.724127	-1.069611	-0.093916
	F	0.737582	1.093639	0.063193		F6	0.612891	1.131179	-0.179930
	F	0.737585	-1.093637	0.063193		Mu7	0.129361	0.067761	1.437152
3	C1	-1.390365	-0.000001	0.045400	3	C1	1.398810	-0.076124	-0.089524
	Mu2	-1.867893	-0.887212	-0.365537		H2	2.168518	0.441779	0.461167
	H3	-1.867895	0.887208	-0.365536		H3	1.630502	-0.569200	-1.021436
	H4	-1.522997	-0.000003	1.134442		C4	-0.003720	0.007169	0.354165
	C5	0.054079	0.000000	-0.302207		F5	-0.621771	1.127120	-0.181110
	F6	0.737582	1.093639	0.063193		Mu6	-0.129516	0.069265	1.436537
	F7	0.737585	-1.093637	0.063193		F7	-0.716012	-1.074688	-0.092681

Table S3. Optimized geometries of reactants and transition states (TS) for reaction channels A–D using several model chemistries and the 6-311++G(3df,3pd) basis set.

VDF

	UB3LYP			UHF			UMP2		
	X	Y	Z	X	Y	Z	X	Y	Z
C1	-0.000005	1.381277	0.000000	-0.000001	1.362756	0.000000	-0.000001	1.382861	0.000000
H2	-0.933824	1.916774	0.000000	-0.927680	1.892562	0.000000	-0.937140	1.908726	0.000000
H3	0.933809	1.916781	0.000000	0.927677	1.892564	0.000000	0.937137	1.908727	0.000000
C4	0.000000	0.066283	0.000000	0.000000	0.060746	0.000000	0.000000	0.062508	0.000000
F5	1.078854	-0.695491	0.000000	1.055088	-0.684784	0.000000	1.076140	-0.693870	0.000000
F6	-1.078849	-0.695499	0.000000	-1.055087	-0.684786	0.000000	-1.076139	-0.693871	0.000000

TSA

	UB3LYP			UHF			UMP2		
	X	Y	Z	X	Y	Z	X	Y	Z
C1	1.306323	-0.000026	-0.243279	1.315654	-0.000004	-0.174723	-1.311609	-0.000014	-0.164083
H2	1.828715	-0.933207	-0.362224	1.819779	-0.924370	-0.355937	-1.817470	0.932626	-0.336952
H3	1.828740	0.933140	-0.362241	1.819782	0.924360	-0.355941	-1.817454	-0.932665	-0.336937
C4	-0.005105	-0.000004	-0.075082	-0.018710	-0.000001	-0.092353	0.003576	-0.000001	-0.074502
F5	-0.752153	1.078917	0.043939	-0.744877	1.062916	0.039321	0.746315	-1.073340	0.032796
F6	-0.752193	-1.078894	0.043950	-0.744883	-1.062912	0.039322	0.746293	1.073353	0.032792
Mu7	2.074347	0.000032	1.843630	1.986609	0.000003	1.606540	-1.950358	0.000017	1.515099

TSB

	UB3LYP			UHF			UMP2		
	X	Y	Z	X	Y	Z	X	Y	Z
C1	-0.054067	-0.000002	0.022613	0.041956	0.000000	0.058509	0.054951	0.000000	0.037017
C2	-1.384206	-0.000007	-0.090831	1.381476	0.000000	-0.094931	1.375077	0.000000	-0.086588
H3	-1.917402	0.935116	-0.080698	1.909543	-0.928795	-0.075814	1.900836	-0.936844	-0.079097
H4	-1.917401	-0.935130	-0.080689	1.909543	0.928795	-0.075814	1.900837	0.936843	-0.079097
F5	0.695887	1.082884	-0.074900	-0.686401	-1.063541	-0.086627	-0.691114	-1.078183	-0.072389
F6	0.695900	-1.082878	-0.074900	-0.686401	1.063541	-0.086627	-0.691114	1.078183	-0.072388
Mu7	-0.061639	0.000007	1.918888	-0.004467	0.000000	1.929446	0.058213	-0.000001	1.758618

TSC

	UB3LYP			UHF			UMP2		
	X	Y	Z	X	Y	Z	X	Y	Z
C1	0.000000	0.083541	0.000000	0.000000	0.076719	0.000000	0.000000	0.084624	0.000000
C2	1.296533	-0.066691	0.000000	1.265897	-0.246635	0.000000	1.283785	0.103579	0.000000
H3	1.781587	-1.551885	0.000000	1.549221	-1.634099	0.000000	1.884156	-1.303417	0.000000
H4	2.101342	0.643100	0.000000	2.100500	0.416697	0.000000	1.993086	0.905248	0.000000
F5	-0.882519	-0.898706	0.000000	-0.981555	-0.762312	0.000000	-0.743889	-0.995295	0.000000
F6	-0.639118	1.247410	0.000000	-0.457944	1.287806	0.000000	-0.785286	1.142832	0.000000
Mu7	2.032600	-2.330646	0.000000	1.710388	-2.492552	0.000000	2.182628	-2.058884	0.000000

TSD

	UB3LYP			UHF			UMP2		
	X	Y	Z	X	Y	Z	X	Y	Z
C1	-0.976908	1.115842	0.000000	-0.982475	1.110860	0.000000	-0.958612	1.105429	0.000000
H2	-0.763892	2.177352	0.000000	-0.780594	2.165232	0.000000	-0.731034	2.162673	0.000000
H3	-1.998889	0.775533	0.000000	-1.992080	0.760000	0.000000	-1.977947	0.763652	0.000000
C4	0.000000	0.250002	0.000000	0.000000	0.252332	0.000000	0.000000	0.255263	0.000000
Mu5	-0.445956	-2.599358	0.000000	-0.410326	-2.598916	0.000000	-0.441111	-2.479902	0.000000
F6	-0.279860	-1.375241	0.000000	-0.257365	-1.393879	0.000000	-0.291639	-1.351013	0.000000
F7	1.287658	0.425397	0.000000	1.266015	0.448828	0.000000	1.280725	0.394282	0.000000

Table S4. Computed activation parameters for the gas phase $^{0.11}\text{H} + \text{VDF}$ reaction using several model chemistries.

UB3LYP Model Chemistry

Reaction	ΔH^\ddagger (kJ mol $^{-1}$)	ΔG^\ddagger (kJ mol $^{-1}$)	ΔS^\ddagger (J mol $^{-1}$ K $^{-1}$)	k/k_{\max}
A	3.10	26.00	-76.83	1.00
B	24.98	49.27	-81.47	8.39×10^{-5}
C	92.37	113.17	-69.76	5.35×10^{-16}
D	147.22	168.29	-70.66	1.18×10^{-25}

UHF Model Chemistry

Reaction	ΔH^\ddagger (kJ mol $^{-1}$)	ΔG^\ddagger (kJ mol $^{-1}$)	ΔS^\ddagger (J mol $^{-1}$ K $^{-1}$)	k/k_{\max}
A	32.58	55.93	-78.33	1.00
B	48.48	72.32	-79.98	1.34×10^{-3}
C	138.69	160.77	-74.04	4.29×10^{-19}
D	269.19	289.84	-69.28	1.04×10^{-41}

UMP2 Model Chemistry

Reaction	ΔH^\ddagger (kJ mol $^{-1}$)	ΔG^\ddagger (kJ mol $^{-1}$)	ΔS^\ddagger (J mol $^{-1}$ K $^{-1}$)	k/k_{\max}
A	52.97	77.26	-81.46	1.00
B	74.49	99.05	-82.39	1.52×10^{-4}
C	157.70	179.59	-73.42	1.18×10^{-18}
D	231.82	252.59	-69.67	1.91×10^{-31}

The results of methods (1) and (2) agree with the conclusion that reaction pathway follows A and that the primary muoniated VDF radical is that in which muonium has added to VDF's protonated carbon.

Critical Slowing and Activation Volumes

In establishing an expression to describe the pressure dependence of k , a minimal number of parameters were desired. Our primary interest lay with describing the declining reaction rate as $P \rightarrow P_{\max}$. From the work in^[S21] it has been reported that for critically slowed reactions, measured rates of reaction vanish proportional to $|(T-T_c)/T_c|^\gamma$, where T is the absolute temperature, T_c is the critical temperature, and γ is the critical exponent. Our analysis attempts to extend this understanding to reactions at isothermal conditions. Hence, in our description in the pressure dependence of k , we include an analogous factor $|(P-P_{\max})/P_{\max}|^\gamma$, where P is pressure, P_{\max} is the pressure where compressibility is at its maximum, and γ is the critical exponent. Several analogous expressions to Eq. 2 were used in an attempt to describe the observed pressure dependence of $^{0.11}\text{H} + \text{VDF}$ rate coefficients:

$$k = A \exp(\alpha P) \left| \frac{P - P_{\max}}{P_{\max}} \right|^\gamma \quad (4)$$

$$k = \exp(a + bP + cP^2) \left| \frac{P - P_{\max}}{P_{\max}} \right|^\gamma \quad (5)$$

wherein the aforementioned expression in Eq. 2 produced minimal χ^2 fits to our data. Fig. S4 shows fits of all three rate functions to our data. Tab. S5 gives the optimized fit parameters for Eq. 2.

A in our expression describing the pressure dependence of rate coefficients (Eq. 2) was to account for the effect of the low pressure rate of the description of critical slowing of the reaction. From the optimized parameters in Tab. S5, it can be seen that for isotherms where critical slowing is observed, fits were insensitive to its inclusion as a fit parameter. However, when critical slowing begins to vanish, its presence becomes more meaningful. While it is unlikely that A provides an accurate zero-pressure rate (as none of our data is within the low pressure reaction limit), it is helpful in identifying a transition in rate behaviour at different isotherms.

As is demonstrated in Fig. S5, each expression describes the behaviour in regions of slowing as being model-independent. Therefore, our observed trends of activation volumes are based on experimental pressure dependence of rate constants, with no dependence on any model used for fitting to the data. The experimental gradients of $\ln k$ with respect to pressure have also been investigated for computation of activation volumes and in all cases produced similar values to those shown in Fig. 5.

Table S5. Optimized fit parameters of Eq. 2 for the isothermal pressure dependence of the $^{0.11}\text{H} + \text{VDF}$ reaction in CO_2 .

T (K)	A ($\text{M}^{-1} \text{s}^{-1}$)	α ($\text{M}^{-1} \text{s}^{-1} \text{bar}^{-1}$)	γ	P_{\max} (bar)	P (EOS) ^a
304.29 ± 0.05	$(0 \pm 4) \times 10^7$	$(1.66 \pm 0.09) \times 10^7$	0.183 ± 0.021	74.0 ± 0.6	74.045
318.18 ± 0.10	$(5.7 \pm 0.5) \times 10^8$	$(8.6 \pm 1.1) \times 10^7$	1.13 ± 0.22	85 ± 4	93.999
333.23 ± 0.16	$(6.3 \pm 0.4) \times 10^8$	$(1.04 \pm 0.12) \times 10^{-3}$	3.386 ± 0.017	0.285 ± 0.009^b	103.315

^aPressures correspond to values of maximum isothermal compressibility determined using the EOS

^bThe nonsensical nature of this globally optimized fit parameter is indicative of no observable critical slowing at this isotherm. This is expected, as the temperature is significantly greater than CO_2 's critical temperature.

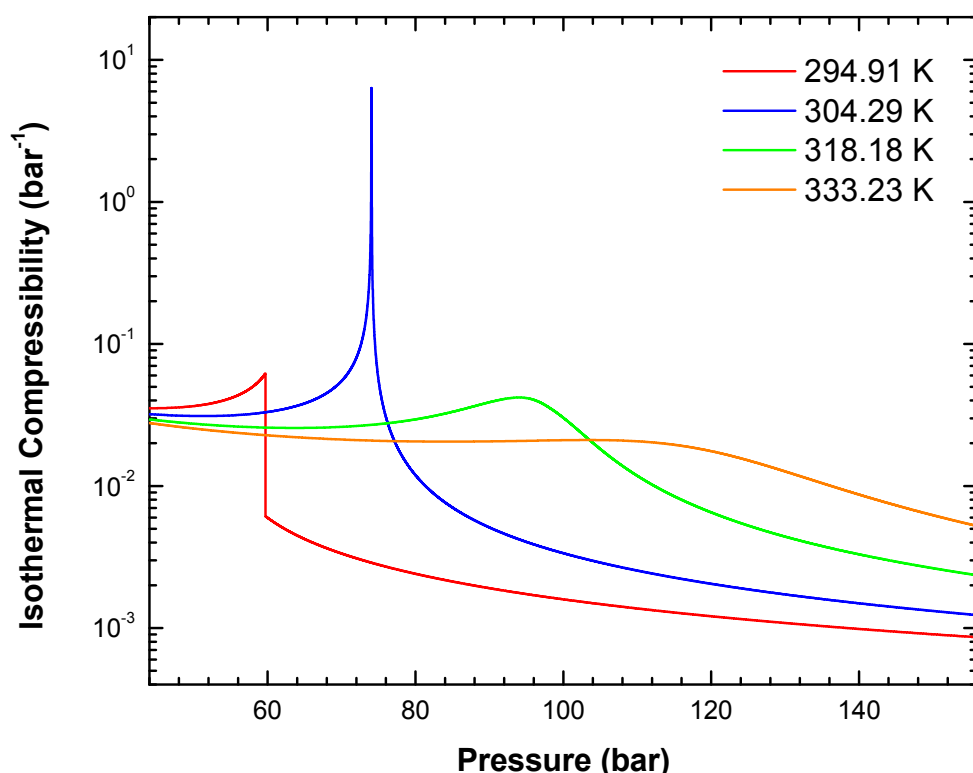


Figure S4. Isothermal compressibility of CO_2 using the equation of state in (S3).

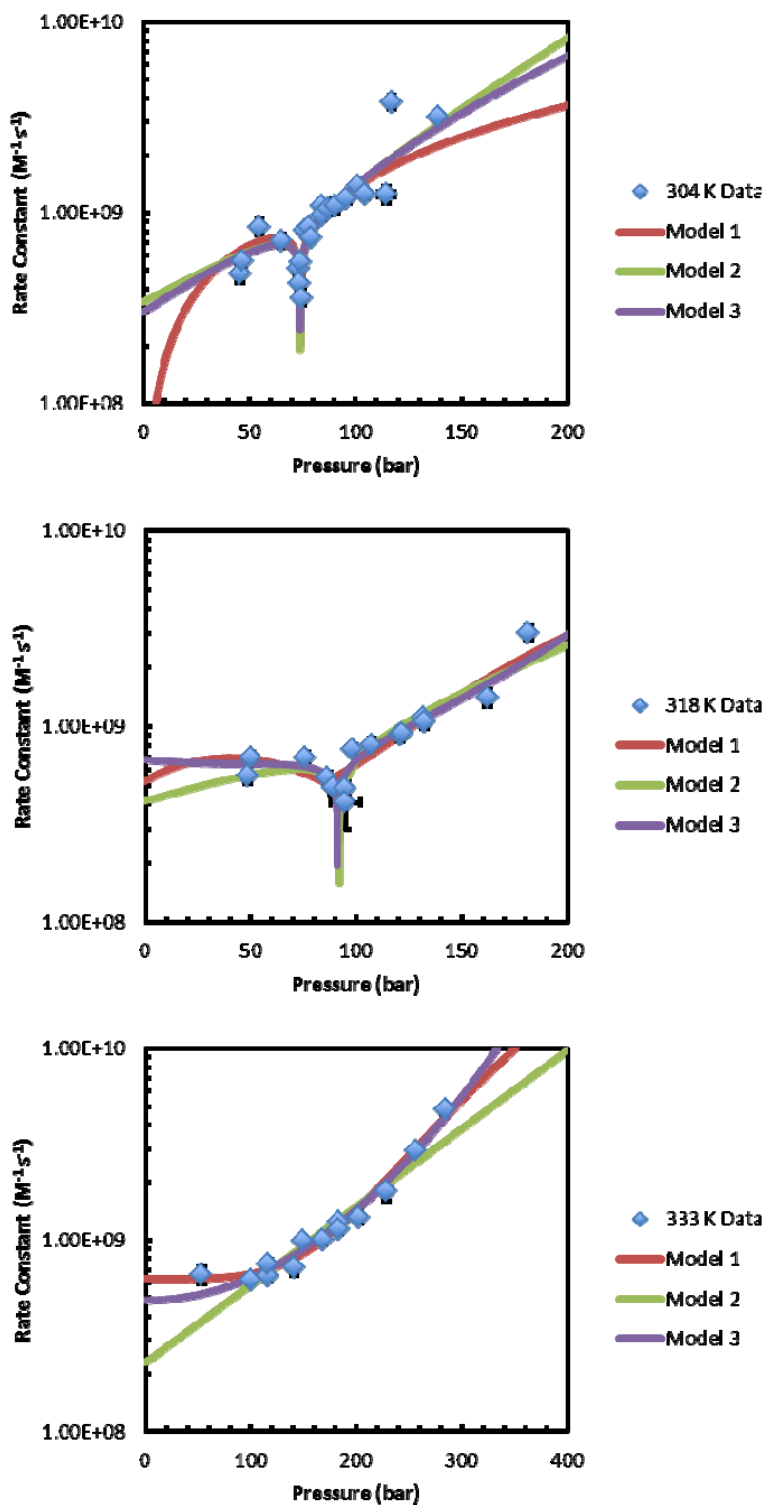


Figure S5. ^{304}K ^{318}K and ^{333}K $^{304}\text{H} + \text{VDF}$ pressure dependence fits using Eq. 1 (Model 1), Eq. 4 in ESI (Model 2), and Eq. 5 in ESI (Model 3).

References

- [S1] K. Ghandi, M. D. Bridges, D. J. Arseneau, D. G. Fleming, Muonium formation as a probe of radiation chemistry in sub- and supercritical carbon dioxide. *J. Phys. Chem. A* **2004**, *108*, 11613–11625.
- [S2] J.-C. Brodovitch, Apparatus for μ SR and μ LCR experiments on fluids at high pressure and temperature. *Physica B* **2006**, *374*–*375*, 314–316.
- [S3] R. Span, W. Wagner, A new equation of state for carbon dioxide covering the fluid region from the triple-point temperature to 1100 K at pressures up to 800 MPa. *J. Phys. Chem. Ref. Data* **1996**, *25*, 1509–1596.
- [S4] M. J. Frisch, G. W. Trucks, H. B. Schlegel, G. E. Scuseria, M. A. Robb, J. R. Cheeseman, G. Scalmani, V. Barone, B. Mennucci, G. A. Petersson, H. Nakatsuji, M. Caricato, X. Li, H. P. Hratchian, A. F. Izmaylov, J. Bloino, G. Zheng, J. L. Sonnenberg, M. Hada, M. Ehara, K. Toyota, R. Fukuda, J. Hasegawa, M. Ishida, T. Nakajima, Y. Honda, O. Kitao, H. Nakai, T. Vreven, J. A. Montgomery, Jr., J. E. Peralta, F. Ogliaro, M. Bearpark, J. J. Heyd, E. Brothers, K. N. Kudin, V. N. Staroverov, R. Kobayashi, J. Normand, K. Raghavachari, A. Rendell, J. C. Burant, S. S. Iyengar, J. Tomasi, M. Cossi, N. Rega, J. M. Millam, M. Klene, J. E. Knox, J. B. Cross, V. Bakken, C. Adamo, J. Jaramillo, R. Gomperts, R. E. Stratmann, O. Yazyev, A. J. Austin, R. Cammi, C. Pomelli, J. W. Ochterski, R. L. Martin, K. Morokuma, V. G. Zakrzewski, G. A. Voth, P. Salvador, J. J. Dannenberg, S. Dapprich, A. D. Daniels, Ö. Farkas, J. B. Foresman, J. V. Ortiz, J. Cioslowski, and D. J. Fox, Gaussian 09, Revision A.1, Gaussian, Inc., Wallingford CT, **2009**.
- [S5] A. D. Becke, Density-functional thermochemistry. III. The role of exact exchange. *J. Chem. Phys.* **1993**, *98*, 5648–5652.
- [S6] V. Barone, in *Recent Advances in Density Functional Methods*, D. P. Chong, Ed. (World Scientific, Singapore, 1996), chapt. 8, pp. 287–334.
- [S7] P. Cormier, D. J. Arseneau, J. C. Brodovitch, J. M. Lauzon, B. A. Taylor, K. Ghandi, Free radical formation in supercritical CO₂, using muonium as a probe and implication for H atom reaction with ethene. *J. Phys. Chem. A* **2008**, *112*, 4593–4600.
- [S8] P. M. Scott, K. R. Jennings, Addition of hydrogen atoms to vinyl fluoride, 1,1-difluoroethylene, and trifluoroethylene. *J. Phys. Chem.* **1969**, *73*, 1521–1525.
- [S9] R. D. Penzhorn, H. L. Sandoval, Addition and abstraction reaction of thermal hydrogen atoms with fluorinated ethylenes. *J. Phys. Chem.* **1970**, *74*, 2065–2073 (1970).
- [S10] L. Teng, W. E. Jones, Kinetics of the reaction of hydrogen atoms with 1,1-difluoroethylene. *J. Chem. Soc., Faraday Trans. 1* **1973**, *69*, 189–197.
- [S11] C. C. J. Roothan, New developments in molecular orbital theory. *Rev. Mod. Phys.* **1951**, *23*, 69–89.
- [S12] J. A. Pople, R. K. Nesbet, Self-consistent orbitals for radicals. *J. Chem. Phys.* **1954**, *22*, 571–572.
- [S13] R. McWeeny, G. Dierksen, Self-consistent perturbation theory II. extension to open shells. *J. Chem. Phys.* **1968**, *49*, 4852–4856.
- [S14] C. Møller, M. S. Plesset, Note on the approximation treatment for many-electron systems. *Phys. Rev.* **1934**, *46*, 618–622.
- [S15] M. Head-Gordon, J. A. Pople, M. J. Frisch, MP2 energy evaluation by direct methods. *Chem. Phys. Lett.* **1988**, *153*, 503–506.
- [S16] S. Saebø, J. Almlöf, Avoiding the integral storage bottleneck in LCAO calculations of electron correlation. *Chem. Phys. Lett.* **1989**, *154*, 83–89.
- [S17] M. J. Frisch, M. Head-Gordon, J. A. Pople, Direct MP2 gradient method. *Chem. Phys. Lett.* **1990**, *166*, 275–280.
- [S18] M. J. Frisch, M. Head-Gordon, J. A. Pople, Semi-direct algorithms for the MP2 energy and gradient. *Chem. Phys. Lett.* **1990**, *166*, 281–289.
- [S19] M. Head-Gordon, T. Head-Gordon, Analytical MP2 frequencies without fifth order storage: theory and application to bifurcated hydrogen bonds in the water hexamer. *Chem. Phys. Lett.* **1994**, *220*, 122–128.

-
- [S20] A. Fernández-Ramos, J. A. Miller, S. J. Klippenstein, D. G. Truhlar, Modeling the kinetics of bimolecular reactions. *Chem. Rev.* **2006**, *106*, 4518–4584.
 - [S21] I. Procaccia, M. Gitterman, Slowing down of chemical reactions near thermodynamic critical points. *Phys. Rev. Lett.* **1981**, *46*, 1163–1166.